frontiers | Frontiers in Earth Science

TYPE Original Research
PUBLISHED 12 August 2022
DOI 10.3389/feart.2022.965898

OPEN ACCESS

EDITED BY
Jinan Guan,
Guangzhou Institute of Energy Conversion (CAS), China

REVIEWED BY
Junqian Li,
China University of Petroleum, China
Zhonggui Hu,
Sequence stratigraphy, China

*CORRESPONDENCE
Feng Changmao,
fengchangm@163.com
Wang Yanlin,
wenhuiwen@163.com

SPECIALTY SECTION
This article was submitted to Marine Geoscience, a section of the journal Frontiers in Earth Science

RECEIVED 10 June 2022
ACCEPTED 05 July 2022
PUBLISHED 12 August 2022

CITATION
Guangjian Z, Changmao F, Yanlin W, Shenghong C, Ming S, Hai Y, Junhui Y, Jing Z and Zhongquan Z (2022), Fault-bounded models of oil–Gas and gas–Hydrate accumulation in the Chaoshan Depression, the South China Sea.
Front. Earth Sci. 10:965898.
doi: 10.3389/feart.2022.965898

Fault-bounded models of oil–Gas and gas–Hydrate accumulation in the Chaoshan Depression, the South China Sea

Zhong Guangjian[1,2], Feng Changmao[1]*, Wang Yanlin[2,3]*, Chen Shenghong[1], Sun Ming[1], Yi Hai[1], Yu Junhui[2,3], Zhao Jing[1] and Zhao Zhongquan[1]

[1]Guangzhou Marine Geological Survey, Guangzhou, China, [2]Southern Marine Science and Engineering Guangdong Laboratory (Guangzhou), Guangzhou, China, [3]Key Laboratory of Ocean and Marginal Sea Geology, South China Sea Institute of Oceanology, Innovation Academy of South China Sea Ecology and Environmental Engineering, Chinese Academy of Sciences, Guangzhou, China

The Dongsha Basin is a large Mesozoic basin extended from the northern South China Sea (SCS) to onshore South China. Though long-term uplift and denudation occurred since the end of the Mesozoic, still thick Mesozoic strata (up to 5,000 m) relict over the Dongsha waters where lies the largest depression, Chaoshan Depression, covering an area of 3.7×10^4 km^2. It was confirmed by a drilling hole, the well LF35-1-1, that high organic carbon-bearing marine Jurassic layers are present in the depression. However, due to the complexity of the superposed Mesozoic and Cenozoic tectonism and poor imaging quality in previous surveys, the petroleum geology remains poorly understood in view of the deep basin structure, the Mesozoic hydrocarbon migration conditions, and the oil–gas accumulation mechanism. In recent surveys, the seismic imaging quality has been significantly improved by employing long and quasi-3D seismic streamer techniques. Correlating with the regional geology onshore the South China, drilling data of the Well LF35-1-1, and well-tying seismic profiles, it is found that two sets of source rocks are developed in the semi-closed gulf during the Upper Triassic-Lower Jurassic and the Upper Jurassic. Their effective thicknesses are estimated as 495 m and 600 m, respectively, being hopeful with high hydrocarbon generation potentials. During the Dongsha Movement that occurred in the late Cenozoic, deep faults have been extensively activated to disturb the overlying sequences, even in some places breaking through the seafloor. A potential trap structure, DS-A, is found in an intra-sag bulge which is bounded by antithetic and synthetic faults. The oil and gas generated in the neighboring sags can migrate along the faults into reservoir layers at higher levels. The antithetic faults also play the role of seal for oil and gas from the hanging wall. Apparent flat bright spots appearing within the DS-A trap indicate likely entrapment of layered petroleum. The synthetic faults on the opposite side of the DS-A structure, although fails to seal oil–gas reservoirs, provide plumbing channels for oil and gas to leak to the shallow layers above which a few pockmarks and mud volcanoes are visible. As the water depth of the continental slope there ranges from 300 m to 2000 m, it is likely for the leaked gas to form natural gas hydrates. A close cogenetic interrelation exists

between the natural gas hydrates at the seafloor and oil–gas reservoirs in the deep.

KEYWORDS

the South China Sea, the Chaoshan Depression, the Mesozoic, tectonic evolution, fault-bounded model, oil–gas accumulation, fault-leakage model, gas–hydrate accumulation

Introduction

Gas hydrate can occur in various morphologies, such as massive, veiny, nodular, and distributive (Lee and Collett, 2009; Bahk et al., 2011; Boswell et al., 2012; Wu et al., 2013; Su et al., 2014, 2020; Liu et al., 2015, 2017; Liang et al., 2016). There are three genetic models of gas hydrate reservoirs, i.e., diffusive model, seeping model, and mixed model depending on whether porosity or fracture operates dominantly in the accumulation process. The gas source of hydrate can be biogenic limited in shallow sedimentary layers or thermogenic hydrocarbon leaked from deep substrates, often oil and gas reservoirs. In terms of potential and higher efficiency in joint exploration and production, the cogenetic gas of hydrate and petroleum has become more attractive.

Hydrates have been discovered over numerous sites in the Cenozoic sedimentary basins (such as the Pearl River Mouth Basin) in the northern SCS. The Chaoshan Depression is the largest Mesozoic depression of the Dongsha Basin bordering the southeast of the Pearl River Mouth Basin, but neither oil–gas nor gas–hydrate have yet been discovered. The drilling results confirmed thin Cenozoic is underlain by thick Mesozoic strata which comprise marine source rock layers. However, the conditions for the formation of hydrates in the Chaoshan Depression have been not clearly expounded. Due to the deep burial of the Mesozoic source layers, it was difficult to clearly reveal the sedimentary filling structure and tectonic deformation characteristics of the basin by poorly imaged seismic reflection in the past. In recent surveys, the Guangzhou Marine Geological Survey (GMGS) has used long and quasi-3D seismic streamers in surveys, which significantly improved the imaging quality of the seismic profiles, revealed the Mesozoic strata in the middle and deep layers more clearly than before, enabling more understanding of the Mesozoic geological structure and petroleum geological conditions of the depression. Based on the latest survey data, it is found that there is a large trap structure (**DS-A** structure) in the low bulge in the central Chaoshan Depression, bounded by antithetic and synthetic faults, which may provide favorable conditions for the formation of oil–gas and hydrates, respectively.

Geological setting

The outcrops onshore South China provinces confirm that a far-reaching transgression began in the early Late Triassic ($\mathbf{T_3^1}$), forming the "Eastern Guangdong Basin" spanning central Guangdong, eastern Guangdong, northern Guangdong, western Fujian, and southern Jiangxi. It was connected with the Dongsha Basin in the northern part of SCS in an advancing trend from sea to land. At the end of the Late Triassic ($\mathbf{T_3^3}$), a brief regression occurred in the East Guangdong Basin. However, in the Early Jurassic, a larger transgression occurred in the East Guangdong Basin, where several hundred meters to nearly 3,000 m of carbonate rocks, clastic rocks, and coal-bearing rock series were deposited. Eastern Guangdong Basin extended to SCS is called Dongsha basin. In the Mid-Late Jurassic, seawater retreated to the northeastern part of SCS, and Mesozoic marine sequences were deposited as evidenced by drill wells in many areas, such as Early Cretaceous marine strata in Well CFC-1 in the central southwestern uplift of Taiwan Basin (Liu, 2001), Mid-Late Jurassic marine strata and Early Cretaceous coastal strata in Well LF35-1-1 on the north slope of Chaoshan Depression (Shao et al., 2007; Wu et al., 2007; Hao et al., 2009). The Mesozoic basins have the characteristics of multi-stage basin formation and multi-stage transformation and are largely superimposed basins formed after the superposition of prototype basins with different evolution characteristics (Zhong et al., 2011).

The Mesozoic basin has experienced long-term structural uplift since the Late Mesozoic and dwindled in the land and sea area in the form of residual depression. Nevertheless, there is a large Mesozoic depression around Dongsha Island where thicker Mesozoic strata are well preserved. The Chaoshan Depression is located on the southeastern side of the Pearl River Mouth Basin in the northern SCS (Figure 1A) covering an area of over 3.7×10^4 km^2. It is the largest Mesozoic residual depression in the northeastern SCS. The Well LF35-1-1 encountered the Mesozoic, of which 1,005m–1369 m is the Cretaceous sand-mudstone section, and 1,369m–1698 m is the Cretaceous tuff section. The 1,698m–2412 m is the Jurassic sand-mudstone section, of which the 1698m–1940m well section is gray–black lamellar mudstone and argillaceous siltstone intercalated with siliceous rock, contains a small amount of micrite limestone, and the rock contains volcanic clastic material; 1940m ~ 2412 m section is composed of gray–black lamellar mudstone and argillaceous siltstone intercalated with sandstone and limestone, and the mudstone is rich in organic matter debris. Radiolarian fossils were found in the 1716m–1839m well section, indicating the deep-sea environment and the Late Jurassic age. Benthic foraminifera fossils are seen in the 2049m–2112 m well

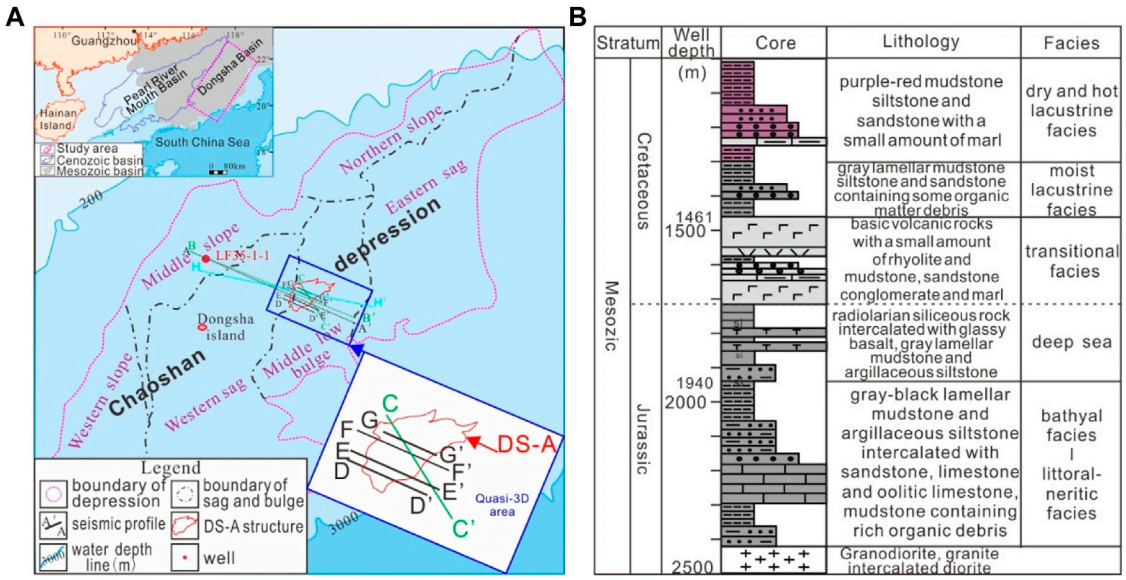

FIGURE 1
Location map and stratigraphic column map. **(A)** Location map of the study area and survey line, structural zoning map of Chaoshan Depression; **(B)** stratigraphic column of well LF35-1-1.

section, indicating this tropical marine shallow water environment. Fossils of sporopollenin can be seen in the 2,187m–2268 m well section, mainly composed of Krassauer and Pseudomonas sporopollenin. This set of sporopollenin fossils appeared in the Middle and Upper Jurassic in southern China, indicating a coastal marsh environment (Shao et al., 2007). Oolitic limestone is seen at 2421 m. Granite-granodiorite intrusions with a small number of diorite intrusions appear in the well section below 2,412 m, and the intrusion period is mainly in the Late Cretaceous (Figure 1B).

Gravity, magnetic and seismic data show weak magmatism over the Chaoshan Depression (Hao et al., 2003). Referring to regional geology, there were mainly two magmatism periods, Yanshanian and Himalayan, respectively. The Himalayan volcanism occurs mainly in the southwest Chaoshan Depression as eruption mainly of intermediate-basic igneous rocks, while the Yanshanian igneous rocks were mainly intrusive in the central and northern slopes as intermediate-acid magmatic rocks (Chen, 2007).

The Chaoshan Depression has experienced weak fracturing in the Late Triassic, depressing in the Jurassic, uplifting in the end Jurassic, rifting in the Cretaceous, uplifting and denudating at the end-Cretaceous, regional thermal subsiding during the Neogene period, and the neo-tectonic Dongsha Movement. The Dongsha Movement occurred at the end of the Middle Miocene and lasted until the early stage of the Late Miocene (Zhao et al., 2012), even to the recent (Yan et al., 2014), leading to the activation of deep faults. It trends generally in the NE direction. Six secondary tectonic units can be divided as the eastern sag, western sag, middle-low uplift, northern slope, central slope, and western slope (Figure 1A). The Mesozoic strata in Chaoshan Depression can be divided into four sequences, $\mathbf{T_3\text{-}J_1}$, $\mathbf{J_2}$, $\mathbf{J_3}$, and **K** (Chen et al., 2005; He et al., 2007, 2013; Shao et al., 2007; Wu et al., 2007; Hao et al., 2009; Feng et al., 2022), developed semi-abyssal-shallow sea ($\mathbf{T_3\text{-}J_1}$), littoral-neritic ($\mathbf{J_2}$), neritic-semi-deep sea ($\mathbf{J_3}$), and sea-land transition-fluvial-lacustrine (**K**) sedimentary layers, the largest in the Mesozoic given the residual sedimentary strata thickness larger than 5000m, it has been deemed resourceful (Wang et al., 2000; Hao et al., 2001, 2004, 2009; Zhou, 2002; Zhou et al., 2003; Zhou et al., 2005; Wang et al., 2009; Duan and Mi, 2012; Zhang et al., 2012; Ji and Zhao, 2014; Hao et al., 2018; Zhang et al., 2018) (Figure 1A).

Data and methods

GMGS has conducted a long array of two-dimensional and quasi-three-dimensional seismic surveys. The most used 2D seismic streamer has 480 channels in 12.5 m spacing. The shooting spacing is 37.5 m using a source capacity of 5,080 cubic inches. The coverage is up to 80-fold.

The seismic data are processed with routine industry procedures and pre-stacked time migration. The focus is on suppression of the turbulence noise, various random noises, linear interferences, and different types of multiples. With the processing, the signals from the shallow, medium, and deep

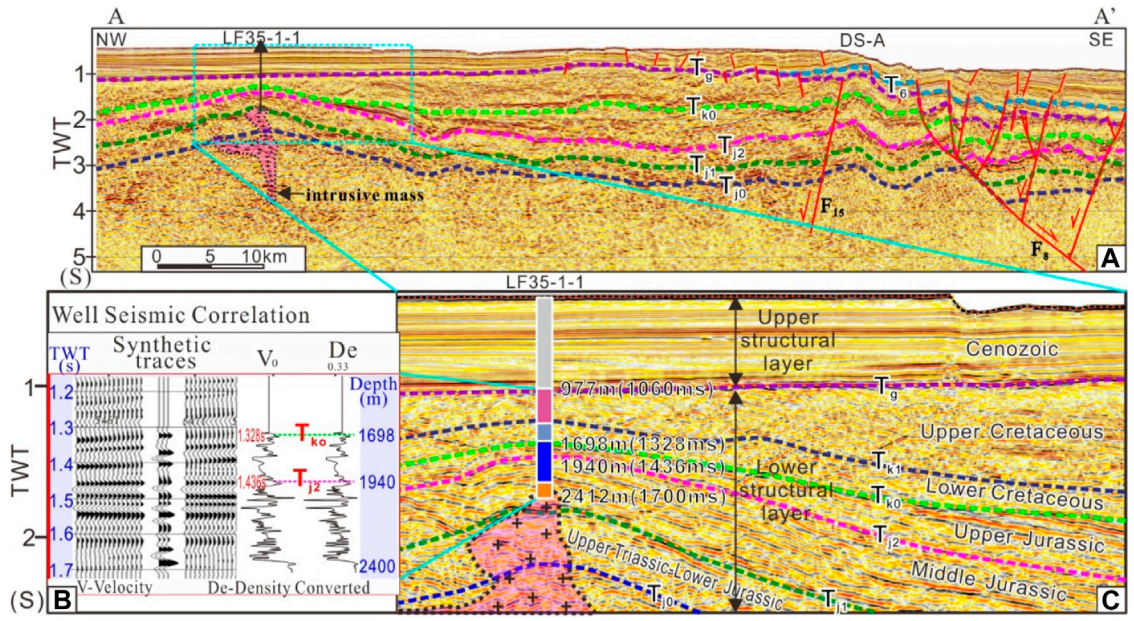

FIGURE 2
Well seismic correlation map. **(A)** Seismic reflection interfaces identified with the Well LF35-1-1; **(B)** well seismic correlation by V and De; **(C)** is the expanded view of **(A)**.

layers are readily discernable, and the wave train characteristics and amplitude characteristics are much clearer than before. The quasi-3D volume regularized with reasonable parameters is also evenly displayed in remarkably enhanced lateral resolution. The improved seismic imaging poses an excellent basis for further analysis of complex geological structures.

The seismic data were interpreted using the GeoFrame software platform. The stratigraphy is interpreted primarily by correlation with the LF35-1-1 well drilled to the north of Dongsha Island (Figure 1A) and analyzed from seismic stratigraphy. Five characteristic seismic reflection interfaces are identified widely over the depression as $\mathbf{T_g}$, $\mathbf{T_{k0}}$, $\mathbf{T_{j2}}$, $\mathbf{T_{j1}}$, and $\mathbf{T_{j0}}$ while the extra two, $\mathbf{T_{k1}}$ and $\mathbf{T_6}$, are identified over local sections (Figure 2).

$\mathbf{T_g}$ is the most obvious unconformity separating the Mesozoic and Cenozoic, which appears at 977 m deep, or two-way time (TWT) of 1,060 ms at the LF35-1-1 column. $\mathbf{T_{k0}}$ is the interface between the Lower Cretaceous and the Upper Jurassic and a strong unconformity interface, its depth is 1698 m corresponding to 1328 ms. $\mathbf{T_{j2}}$ is the interface between the Upper Jurassic and Middle Jurassic with a depth of 1940m corresponding to 1436ms. The upper and lower parts of the interface are in an integrated contact relationship, showing strong reflection characteristics on the seismic profile. $\mathbf{T_{j1}}$ is the interface between the Middle and Lower Jurassic, which has not been revealed by drilling. $\mathbf{T_{j0}}$ is the bottom interface of the Upper Triassic.

Results

One faulted nose structure

Strata over the Chaoshan Depression can be roughly divided on seismic profiles into upper and lower structural layers by the $\mathbf{T_g}$ unconformity (Figure 2). The upper structural layer above shows high-frequency, strong amplitude, and continuous, parallel reflection characteristics, comparable to those in the Pearl River Mouth Basin. The lower structural layer shows low-frequency, medium-weak amplitude, and discontinuous-continuous reflections. It occurs limitedly as an intra-depression deposition, largely in either angularly unconformable or major hiatus contact with the upper layer, indicating that the proto-depression has suffered great uplift and erosion before late subsidence.

The Chaoshan Depression has undergone multi-staged, compressive, and extensional faulting. Compressive faults are only visible in the lower structural layer in limited areal scope, mainly in the northwest and southwest parts. They were active at the end of the Jurassic, usually associated with thrust folding structures. The extensional faults are seen cutting the upper and lower structural layers, more often in the upper structural layer in the continental slope break zone. They fall into three trending groups, i.e., NE, NN, and EW, with the NE-trending faults prevalent over the others (Figure 3A). The extensional faults were active in three periods, the Yanshan Movement to the early

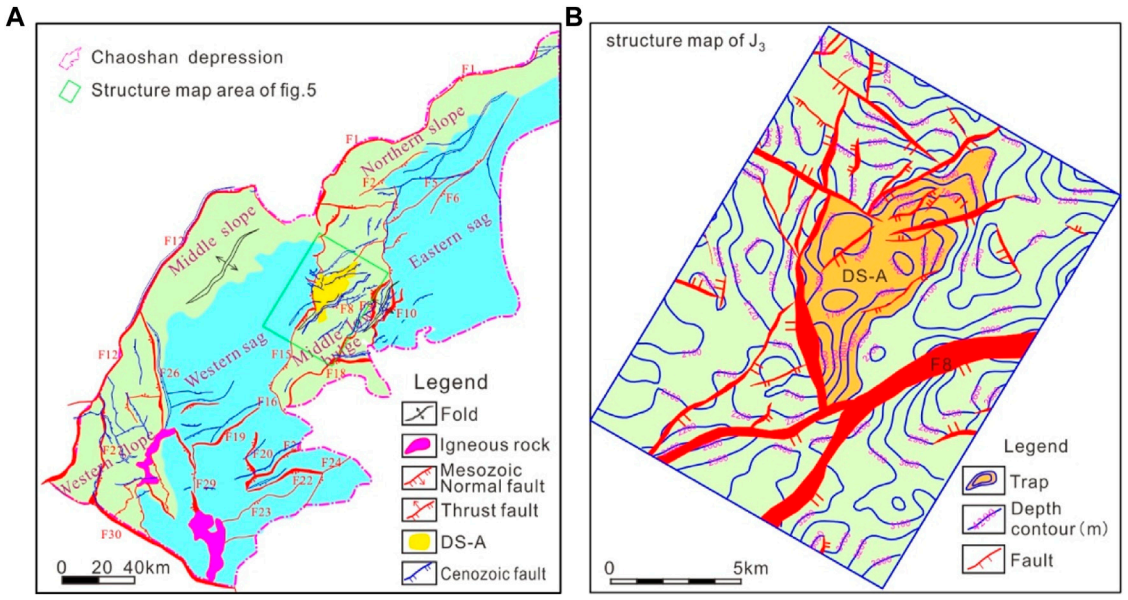

FIGURE 3
Structure map. **(A)** Chaoshan Depression; **(B)** DS-A.

stage of the Himalayan Movement, the late stage of the Himalayan Movement, and the Dongsha Movement (Zhang et al., 2014). The first-stage extensional faults initiated oil–gas migration, while the third-stage faulting can lead to oil–gas leakage from some reservoirs to shallow layers.

A large trap structure, **DS-A**, is found from 2-D profiles and quasi-3D seismic data. It is a fault nose structure composed of multiple fault blocks, fault anticlines, and anticlines. The NE-trending structure is dominated by the wide and gently extruded anticlines, forming a tectonic pattern of alternating uplift and depression belts (Figure 3A). It is located in the west of the central low bulge, covering ~ 300 km^2 (Figure 3B). It began to develop at the end of the Jurassic and was formed in the Late Cretaceous.

Two sets of effective source layers

Two black laminar mudstone intervals between 1940m–2022 m and 2,100m–2400 m in Well LF35-1-1 within the Chaoshan Depression are rich in organic matter. Among them, the thickness of a single mudstone layer in the section from 1940m to 2022 m is generally larger than 6m, with a maximum of 40 m plus and the average at ~20 m. The cumulative thickness of mudstone is 82.28 m. In the mudstones, total organic carbon (TOC) content ranges from 0.18% to 1.15%, averages at 0.67%; HI index ranges from 30 to 118.5 mg/g, with an average of 62.97 mg/g; S1+S2 varies between 0.3–1.71, with an average of 0.98 mg/g; Ro>2.0%; the type of kerogen is mainly of type III, and a few are type II. It is rated as a moderate-good source rock (Figure 4) (Zhong et al., 2007; Yang et al., 2008).

The TOC of the bathyal mudstone of the Shanglongshui Formation (Lower Jurassic) outcropping onshore the South China ranges from 0.5% to 1.71%, with an average of 1.03%, and the TOC of the bathyal mudstone of the Yinpingshan Formation (Lower Jurassic) is 0.64%–1.76%, with an average of 1.31%. The TOC of the neritic-shelf mudstone in the Xiaoshui Formation (Upper Triassic) ranges from 1.17% to 5.43%, with an average of 2.64%. The kerogen types of these three groups are all type II. According to a comprehensive evaluation, source rocks in the Chaoshan Depression can be predicted with great potential for hydrocarbon generation (Zhong et al., 2007).

Correlating the source rock analysis of outcrop on the South China continent and tests of offshore drilling in the Chaoshan Depression, two layers of mudstones deposited in $\mathbf{T_3}$-$\mathbf{J_1}$ bathyal and $\mathbf{J_3}$ neritic—shelf facies are the main source rocks, among which $\mathbf{T_3}$-$\mathbf{J_1}$ source rocks are semi-deep marine facies. The source layers are trustfully established by T well-seismic calibration. They are characteristics of medium-weak amplitude, weak continuity, low frequency, or blank reflection (Figure 4). As a result of seismic interpretation, isopach maps of two effective source layers are compiled. The $\mathbf{T_3}$-$\mathbf{J_1}$ effective source rocks are mainly distributed in the eastern sag, the western sag, and the central low uplift, with a maximum thickness of more than 1000 m and an average thickness of 495 m. The $\mathbf{J_3}$ effective source rocks are mainly distributed in the western sag, with a maximum thickness greater than 1000 m and an average thickness of 600 m (Figure 5).

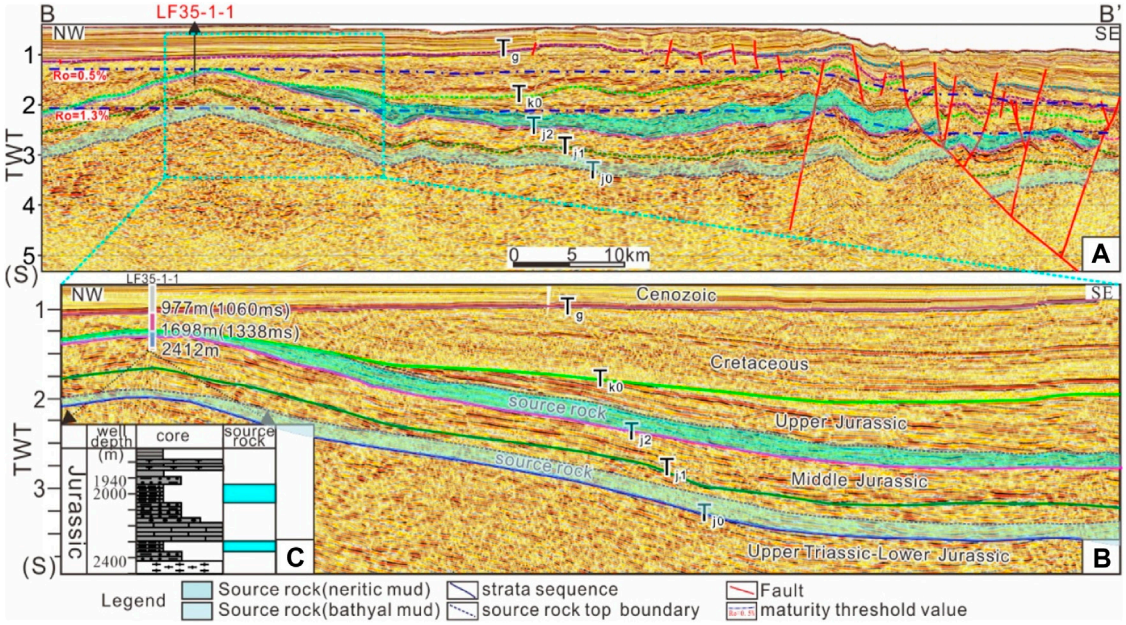

FIGURE 4
Source rocks characteristic of **(A)** two sets of source rocks revealed by seismic, location see Figure 1; **(B)** is the expanded view of **(A)**; **(C)** source rocks revealed by Well LF35-1-1.

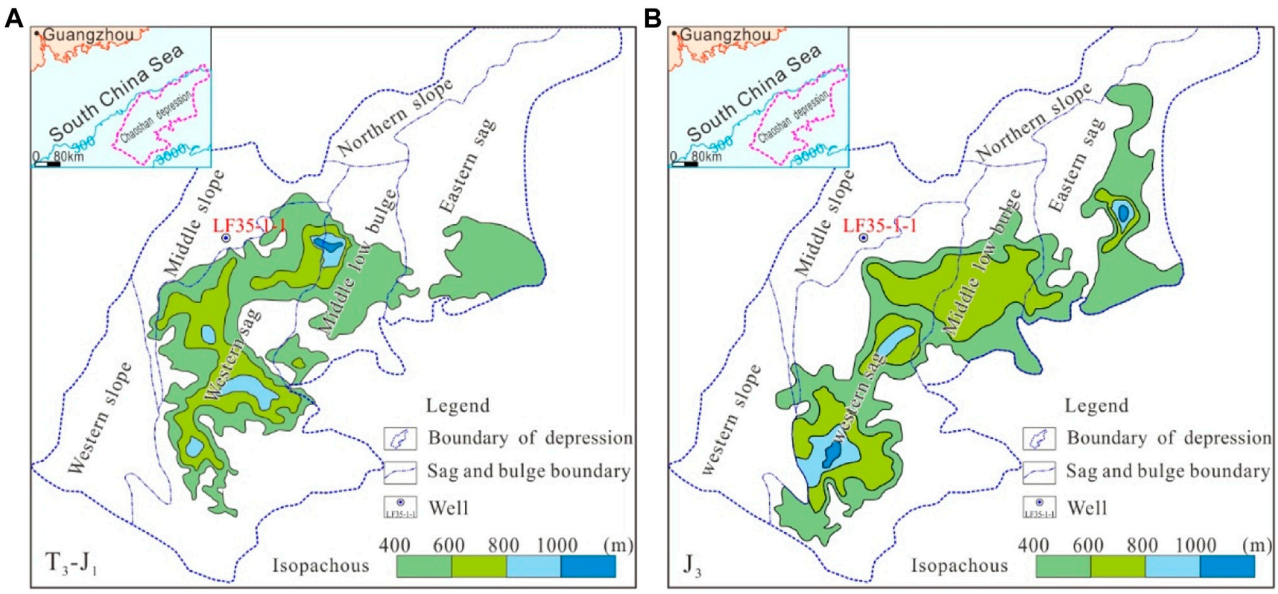

FIGURE 5
Map of mud rock thickness of the two effective source layers in the Chaoshan depression. **(A)** Map of mud rock thickness of T_3-J_1; **(B)** Map of mud rock thickness of J_3.

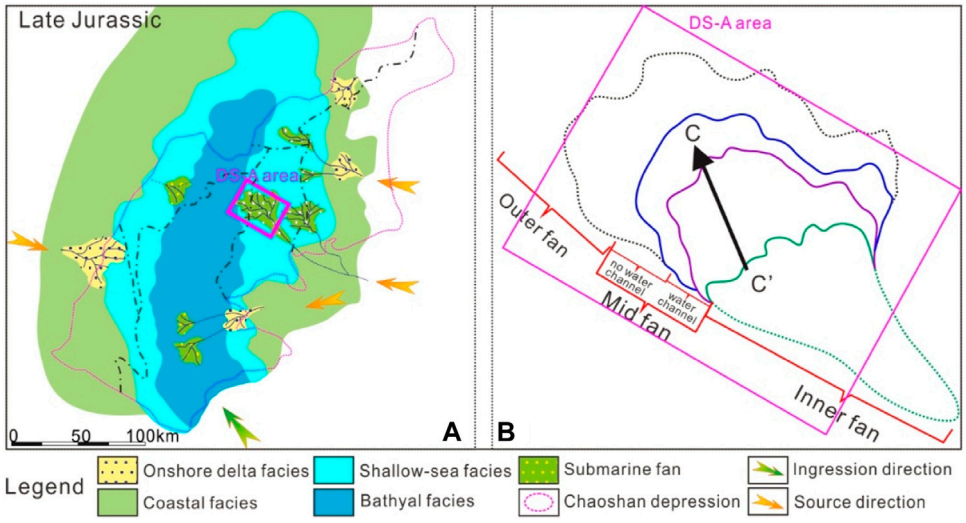

FIGURE 6
Sedimentary facies map in the Chaoshan Depression. **(A)** Map of the Late Jurassic sedimentary facies in the Chaoshan Depression; **(B)** construction of submarine fan.

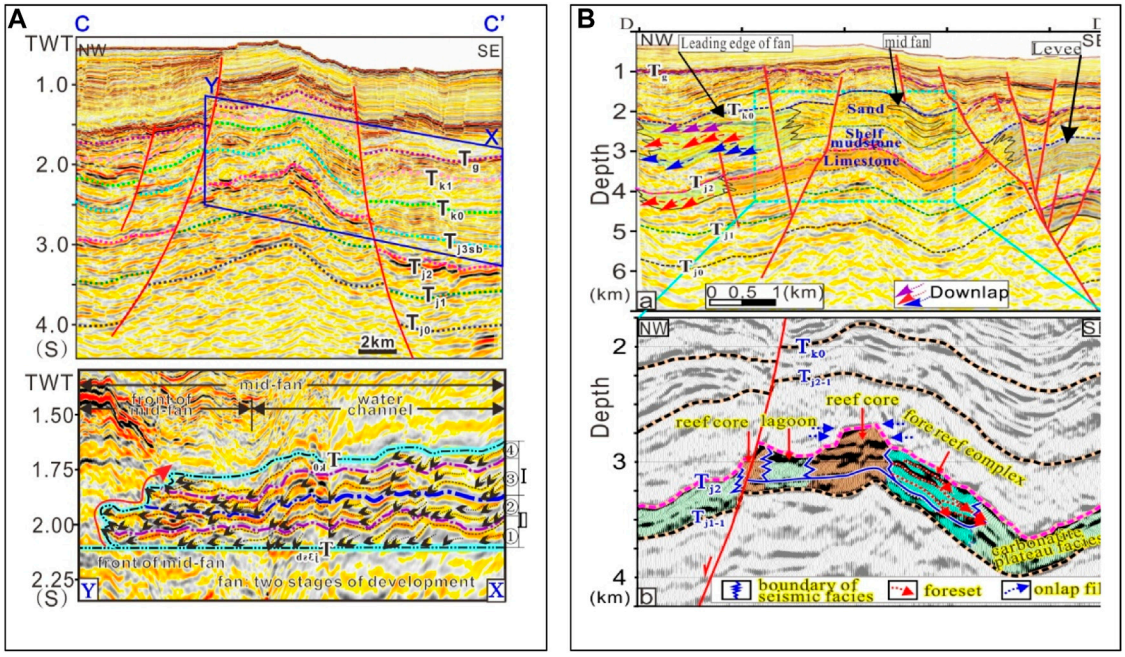

FIGURE 7
Reservoir layer of DS-A, location see Figure 1. **(A)** Interpretation for J_3 fan in DS-A; **(B)** interpretation for J_2 limestone in DS-A.

Three sets of the reservoir layer

There are three sets of reservoirs in the **DS-A** structural area of Chaoshan Depression, i.e., $\mathbf{J_3}$ coastal neritic sandstone, slope fan and submarine fan sandstone, upper $\mathbf{J_2}$ limestone, and $\mathbf{J_{1\text{-}2}}$ sandstone.

At the Well LF35-1-1, the penetrated $\mathbf{J_{2\text{-}3}}$ strata are 714 m thick, in which the total thickness of sandstone is 120 m, and the

maximum thickness of a single layer is 40 m. The sedimentary facies are mainly coastal to deltaic, reef flats, and submarine fans (Figure 6). From the analysis of layer-leveling, sequence stratigraphy, the seismic amplitude attributes of the 3D data volume, and the sand body response characteristics at Well LF35-1-1, a large submarine fan was identified in the upper part of the J_3 in the **DS-A** structure. The bottom of the subsea fan sand body is in sudden contact with the underlying thick bathyal mudstone, and the top is in gradual contact with the overlying thick sea-land transition mudstone, shown by a reflection group of stable and strong amplitude. The prograding features of the sand body along the fan body direction (SE-NW) are clearly visible. The history of the submarine fan can be divided into four stages, of which the second and third stages are the heydays (Figure 7A).

Through well-tied tracking and comparison of the thin layer of oolitic limestone (around 2,421 m) at the top of the Middle Jurassic in Well LF35-1-1, an interface featuring strong amplitude and continuous seismic reflection was traced to below the T_{j2} interface in the **DS-A** structure. The seismic facies between this interface and T_{j2} are blank or sub-parallel weak amplitude reflections (Figure 7B), which can be identified as limestone layers with a thickness of 200m–500 m.

Based on seismic facies analysis, submarine fans were identified in the top of J_3 and the bottom of J_2 in the **DS-A** structure, and a set of stable reflection layers with strong amplitudes appeared in the 3D data volume as a whole, which can be traced continuously. The subsea fan sand is the third set of favorable reservoir rocks in this structure.

Good sealing ability of mudstone

The mudstone encountered in well LF35-1-1 has a large integral thickness, and the maximum thickness of a single layer is greater than 30 m. It should have a good sealing ability and is an important regional cap rock in this area. In addition, many sets of mudstones developed in the Mid-Upper Jurassic, and these mudstones mostly showed continuous or weak continuous, and medium or weak amplitude reflections. By seismic tracking, these mudstones are stable in distribution and can also act as regional cap rocks.

In view of the contact relationship of seismic reflection, it can be found that: 1) **DS-A** structure was completely developed by the early Cretaceous, but suffered strong denudation since the late Cretaceous. The denudation thickness is about 1,100 m; 2) there is no obvious erosion in the Jurassic strata in the **DS-A** structure.

Dual-source and fracture passage

Since the end of the Middle Jurassic, the two sets of source rocks had gradually entered the hydrocarbon generation threshold and had begun to expel hydrocarbons. The **DS-A** structure is adjacent to the western sag on the west side and the eastern sag on the east side. It is a typical intra-sag uplift structure favored with sufficient oil–gas from dual sources for a long duration. There are faults developed in the Mesozoic which cut through the three sets of main source rocks. The oil and gas generated by the Jurassic source rocks in the western and eastern sags can migrate up to J_1 Sandstone, J_2 reef limestone, and J_3 sandstone along the faults, respectively, and multi-layer oil–gas reservoirs finally form at a high point of structural trap (Figure 8). Some Cenozoic faults can further leak the oil and gas to shallow layers. In fact, there are apparent signs of seafloor pockmarks and mud volcanoes around, being indicative of vigorous seep, likely of gas (Figure 9). As the water depth ranges from 300 m to 2000 m, it is highly possible for the leaked gas to form hydrates.

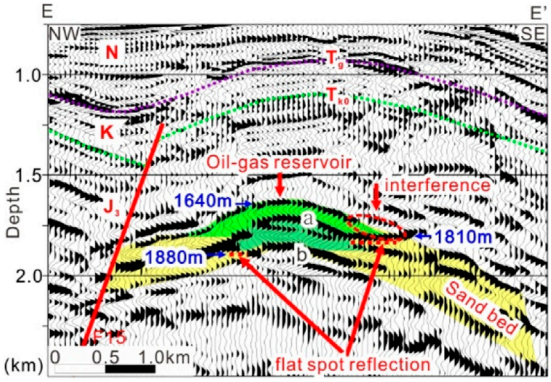

FIGURE 8
Oil–gas reservoir in DS-A.

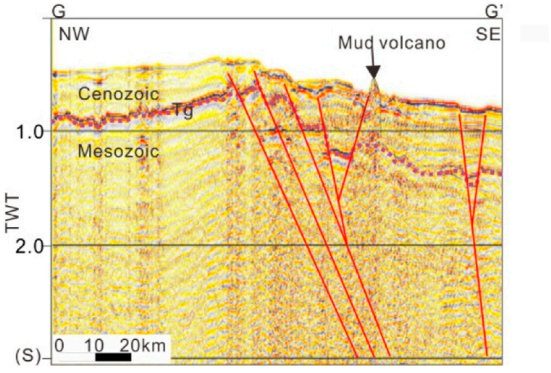

FIGURE 9
Mud volcano nearby DS-A (by courtesy of Yan et al. 2022).

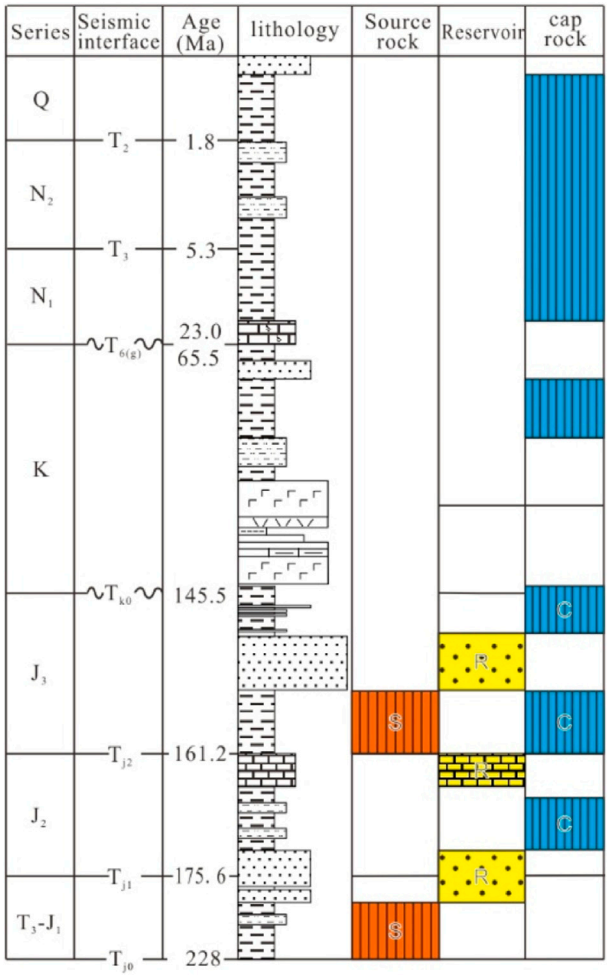

FIGURE 10
Source-reservoir-cap rock combination.

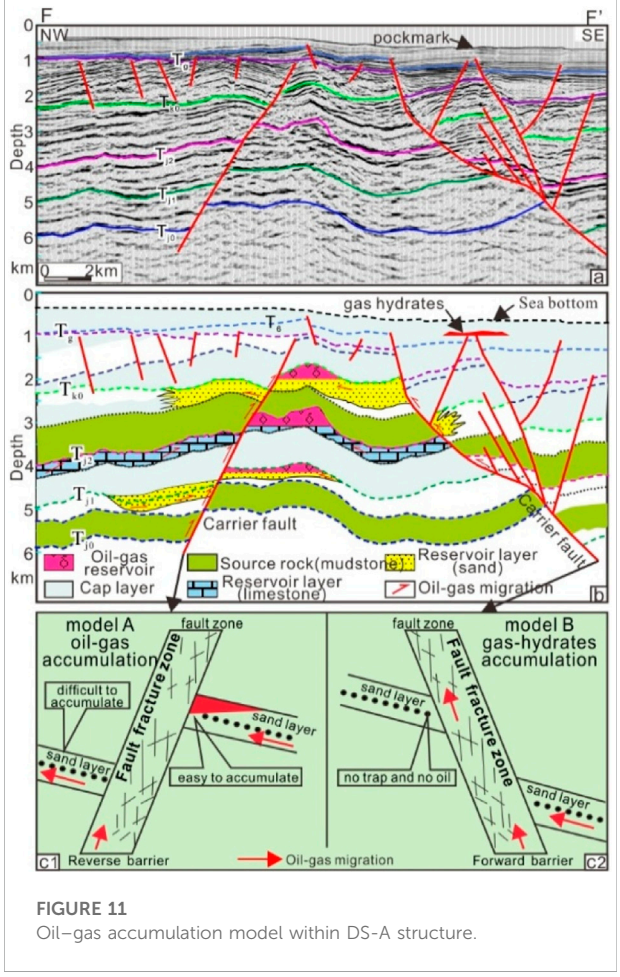

FIGURE 11
Oil–gas accumulation model within DS-A structure.

Discussion

Source-reservoir-cap rock assemblage

According to the mature evolution history of source rocks (Feng et al., 2022), the source rocks at the bottom of the Upper Triassic-Lower Jurassic began to mature at the end of the Late Jurassic, and became highly mature in the middle of the Early Cretaceous. At the same time, the **DS-A** structure began to mature. The source rocks in the lower part of the Upper Jurassic began to mature at the end of the Late Cretaceous, and the **DS-A** structure was established at the same time. At present, all the source rocks in the lower part of the Upper Jurassic have entered high maturity, and the formation of the **DS-A** structural traps has a good relationship with the temporal and spatial configuration of hydrocarbon expulsion and accumulation. According to the tempo-spatial relation (Figure 10), three sets of potentially favorable source-reservoir-cap rock assemblage (**SRCA**) in the Chaoshan Depression can be briefed as 1) $\mathbf{T_3\text{-}J_1}$ bathyal mudstones; J_1 littoral-neritic sandstones; J_2 neritic mudstones; 2) $\mathbf{T_3\text{-}J_1}$ bathyal mudstones; J_3 reef limestone; $\mathbf{J_3}$ neritic and bathyal mudstones; 3) $\mathbf{J_3}$ neritic shelf mudstones; $\mathbf{J_3^2}$—$\mathbf{J_3^3}$ coastal to basin floor fan sand; $\mathbf{J_3}$ neritic and bathyal mudstones.

Antithetic fault-bounded model of oil–gas accumulation

The **DS-A** trap structure started to develop before the peak time of oil–gas migration, fully formed at the end of the Mesozoic when uplift and denudation occurred, and altered during the neotectonics Dongsha Movement. Its formation is accommodated by various faults. Among them, two major faults, antithetic and synthetic, can be recognized as significant for models of potential petroleum reservoir and hydrate accumulation.

The **DS-A** trap sits in the west uptilt flank of a bulged terrain between the Western Sag and the Eastern Sag, which is a typical intra-sag uplift structure. It has developed with two sets of argillaceous source rocks, $\mathbf{T_3}$-$\mathbf{J_1}$ and $\mathbf{J_3}$; the reservoir rocks are submarine fan sand at the top of $\mathbf{T_3}$-$\mathbf{J_1}$ and the bottom of $\mathbf{J_2}$, platform limestone at the top of $\mathbf{J_2}$, and submarine fan sandstone in the middle of $\mathbf{J_3}$. The oil and gas generated in the western and eastern sags can readily migrate along the antithetic faults to accumulate when encountering favorable reservoirs at structural high points over the bulge. In addition, the generated oil and gas can also migrate directly to the upper reservoir through faults (Figure 11). A flat bright spot, ~1 km wide, is visible in Figure 8, which is indicative of a potential layered liquid interface, most likely the realistic existence of gas and oil reservoirs.

Synthetic fault-leakage model of gas-hydrate accumulation

The slope where the Chaoshan Depression sits shows late Cenozoic fault activation. Some of the faults extend from the Mesozoic source rock layers in deep or close to the seafloor, resulting in mud volcanoes (Figure 9) and pockmarks (Figure 11). In fact, much more mud volcanoes have been reported over the Dongsha waters, indicating widespread leakage of oil and gas from the substrates (Yan and Chen, 2009, 2017, 2021; Zhong et al., 2018). As the water depth on the slope ranges from 300 m to 2000 m, the leaked gas can accumulate as a hydrate in the shallow levels (Figure 11, model B).

Conclusion

Based on the latest survey data analysis, Chaoshan Depression has good petroleum geological conditions, and the DS-A structure is a potential trap structure bounded by antithetic and synthetic faults. The oil–gas can migrate along the faults into reservoir layers forming oil–gas reservoir, the oil–gas accumulation is an antithetic fault-bounded model. The synthetic faults provide plumbing channels for oil and gas to form natural gas hydrates, the gas–hydrate accumulation is the synthetic fault-leakage model. A close cogenetic interrelation exists between the natural gas hydrates and oil–gas reservoirs.

1 It can be recognized by seismic correlation with offshore drilling results and onshore outcrops that the main source layers within the Chaoshan Depression comprise the $\mathbf{T_3}$-$\mathbf{J_1}$ and $\mathbf{J_3}$ mudstones, especially, the thick semi-enclosed gulf source rocks of Jurassic which were tested with fairly high organic matter abundance. Three sets of reservoir rock layers are interpreted as, basin-bottom fan sandstone of the Upper Jurassic, limestone of the top mid-Jurassic, and basin floor fan of the upper Lower Jurassic and the bottom Mid-Jurassic. Furthermore, three sets of the source-reservoir-cap assemblage are deemed favorable for petroleum trap **DS-A** within which apparent flat bright spots are visible.

2 The **DS-A** is a nose-shaped structure bounded by antithetic and synthetic faults. It is an intra-sag bulge composed of multiple fault blocks, faulted anticlines, and anticline traps. The faults of different dipping directions play different roles in accumulation models of petroleum and gas hydrates, i.e., the Antithetic Fault-Bounded Model and Synthetic Fault-Leakage Model, respectively. The antithetic faults bounding the uptilt side of the structure displaced the source rock layers in the hanging wall to a low level or contact directly with the sand beds in the footwall, thus enabling source oil and gas to migrate upward or directly into the sand beds reservoir. And the mud smearing along the fault may act as a seal to form reservoirs at high points of the structure.

3 The synthetic faults on the opposite, downdip side of the **DS-A** structure, though incapable of sealing oil–gas reservoirs, provide passages for oil–gas to leak upward to form natural gas hydrates in the shallow layers. Both fault-bounded models are cogenetic in terms of the Mesozoic hydrocarbon sources.

Data availability statement

The original contributions presented in the study are included in the article/supplementary material, further inquiries can be directed to the corresponding authors.

Author contributions

Data processing: ZZ; seismic data interpreting: ZG, FC, and SM; writing-original draft preparation: YH, ZJ, YJ; writing—review and editing: GZ, CF, WY, CS; all authors have read and agreed to the published version of the manuscript.

Funding

Yan Yuning provided a processed seismic profile (Figure 9). Two reviewers are acknowledged for their constructive comments. This research was funded by the National Natural Science Foundation of China (U1901217, 91855101); Key Special Project for Introduced Talents Team of Southern Marine Science and Engineering Guangdong Laboratory (Guangzhou) (GML2019ZD0104, GML2019ZD0201); and Special Support

Program for Cultivating High-level Talents in Guangdong Province (2019BT02H594).

Conflict of interest

The authors declare that the research was conducted in the absence of any commercial or financial relationships that could be construed as a potential conflict of interest.

Publisher's note

All claims expressed in this article are solely those of the authors and do not necessarily represent those of their affiliated organizations, or those of the publisher, the editors, and the reviewers. Any product that may be evaluated in this article, or claim that may be made by its manufacturer, is not guaranteed or endorsed by the publisher.

References

Bahk, J. J., Um, I. K., and Holland, M. (2011). Core lithologies and their constraints on gas-hydrate occurrence in the east sea, offshore korea: Results from the site ubgh1-9. *Mar. Petroleum Geol.* 28 (10), 1943–1952. doi:10.1016/j.marpetgeo.2010.12.003

Boswell, R., Collett, T. S., Frye, M., Shedd, W., McConnell, D. R., and Shelander, D. (2012). Subsurface gas hydrates in the northern Gulf of Mexico. *Mar. Petroleum Geol.* 34 (1), 4–30. doi:10.1016/j.marpetgeo.2011.10.003

Chen, D. F., Su, Z., Feng, D., Lawrence, M. C., et al. (2005). Formation and its controlling factors of gas hydrate reservoir in marine gas vent system. *J. Trop. Oceanogr.* 24 (3), 38–46.

Chen, J. (2007). Geophysical characteristics of the Chaoshan depression and its hydrocarbon exploration potential. *Prog. Geophys.* 22 (1), 147–155.

Duan, J. C., and Mi, H. F. (2012). Seismic facies and sedimentary facies study of mesozoic in chaoshan sag. *Resour. Industries* 14 (1), 100–105. doi:10.13776/j.cnki.resourcesindustries.2012.01.003

Feng, C. M., Zhong, G. J., Sun, M., Lei, Z., Yi, H., and Zhao, Z. (2022). Analysis of the thermogenic gas source of natural gas hydrates over the Dongsha waters in the northern South China sea. *Front. Earth Sci. (Lausanne).* 1, 10. doi:10.3389/feart.2022.873615

Hao, H. J., Lin, H. M., Yang, M. X., Xie, H. Y., and Chen, J. (2001). The mesozoic in chaoshan depression: A new domain of petroleum exploration. *China Offshore Oil Gas (in Chinese)* 15 (3), 157–163.

Hao, H. J., Shi, H. S., Zhang, X. T., Wang, T. C., and Tang, S. L. (2009). Mesozoic sediments and their petroleum geology conditions in chaoshan sag: A discussion based on drilling results from the exploratory well LF35-1-1. *China Offshore Oil and Gas* 21 (3), 151–156.

Hao, H. J., Wang, R. L., Zhang, X. T., Xie, H. Y., and Chen, Z. G. (2004). Mesozoic marine sediment identification and distribution in the eastern Pearl River Mouth Basin. *China Offshore Oil and Gas* 16 (2), 84–88.

Hao, H. J., and Zhang, X. T. (2003). An application of gravimetric and magnetic data in mesozoic petroleum exploration in Chaoshan sag, South China sea. *China Offshore Oil and Gas (Geology)* 17 (2), 128–132.

Hao, H. Y., Zhao, J., Liu, H. S., Zhong, G. J., Ma, W. Y., Xie, P., et al. (2018). Prediction of oil and gas reservoir traps by aromatic hydrocarbons from seabed sediments in Chaoshan depression, South China Sea. *ACTA PETROLEI SINICA* 39 (5), 528–540.

He, J. X., Yan, W., Zhu, Y. H., Zhang, W., Gong, F. X., Liu, S. L., et al. (2013). Biogenetic and sub-biogenetic gas resource potential and genetic types of natural gas hydrates in the northern marginal basins of South China Sea. *Natural Gas Industry* 33 (6), 121–132. doi:10.3787/j.issn.1000-0976.2013.06.023

He, J. X., Yao, Y. J., Ma, W. H., Zhang, S. L., Shi, X. B., Liu, H. L., et al. (2007). Status of oil & gas exploration and analysis of geological character in Mesozoic residual basin, northern South China Sea. *Natural gas geoscience* 18 (5), 635–642.

Ji, Z. Y., Zhao, H. Q., Wang, H. P., and Li, C. L. (2014). The mesozoic petroleum system of chaoshan depression. *Petroleum Geology and Engineering* 28 (3), 9–15.

Lee, M. W., and Collett, T. S. (2009). Gas hydrate saturations estimated from fractured reservoir at Site NGHP-01-10, Krishna-Godavari Basin, India. *J. Geophys. Res.* 114 (B7), B07102. doi:10.1029/2008JB006237

Liang, J. Q., Zhang, G. X., Lu, J. A., Su, P. B., Sha, Z. B., Gong, Y. H., et al. (2016). Accumulation characteristics and genetic models of natural gas hydrate reservoirs in the NE slope of the South China Sea. *Natural Gas Industry* 36 (10), 157–162. doi:10.3787/j.issn.1000-0976.2016.10.020

Liu, C. L., Meng, Q. G., Li, C. F., Sun, J. Y., He, X. L., Yang, S. K., et al. (2017). Characterization of natural gas hydrate and its deposit recovered from the northern slop of the South China Sea. *Earth Science Fronters* 24 (4), 41–50. doi:10.13745/j.esf.yx.2016-12-35

Liu, G. D. (2001). The second exploitation of the oil and gas resources in China. *Progress in Geophysics* 16 (4), 1–3.

Liu, J. L., Wang, S. H., and Yan, W. (2015). Research on coexistence between marine gas hydrate and deep-water oil. *Journal of tropical oceanography* 34 (2), 39–51.

Shao, L., You, H. Q., Hao, H. J., Wu, G. X., Qiao, P. J., Lei, Y. C., et al. (2007). Petrology and depositional environments of mesozoic strata in the northeastern South China sea. *Geological Review* 53 (2), 164–169.

Su, P. B., Liang, J. Q., Zhang, W., Liu, F., Wang, F. F., Li, T. W., et al. (2020). Natural gas hydrate accumulation system in the Shenhu sea area of the northern South China Sea. *Natural Gas Industry* 40 (8), 77–88. doi:10.3787/j.issn.1000-0976.2020.08.006

Su, P. B., Sha, Z. B., Chang, S. Y., Liang, J. Q., Fu, S. Y., et al. (2014). Geological models of gas hydrate formation in the eastern sea area of the Pearl River Mouth Basin. *Natural Gas Industry* 34 (6), 162–168. doi:10.3787/j.issn.1000-0976.2014.06.26

Wang, L. L., Cheng, R. H., Li, F., Zhang, L., and Xu, Z. J. (2009). The mesozoic sedimentary sequences, correlation and geological significance for petroleum of the north margin of South China sea. *Journal of Jilin University (Earth Science Edition)* 39 (2), 175–182. doi:10.13278/j.cnki.jjuese.2009.02.007

Wang, P., Xia, K. Y., and Huang, C. L. (2000). The mesozoic marine sediment distribution and geology-geophysics characteristic at the northeastern of South China continent. *Journal of Tropical Oceanography* 19 (4), 28–35.

Wu, G. X., Wang, R. J., Hao, H. J., and Shao, L. (2007). Microfossil evidence for development of marine Mesozoic in the north of South China Sea. *Marine Geology & Quaternary Geology* 27 (1), 79–85.

Wu, N. Y., Zhang, G. X., Liang, J. Q., Su, Z., Wu, D. D., Lu, H. L, et al. (2013). Progress of gas hydrates research in northern South China Sea. *Adv. New Renew. Energies.* 1 (1), 80–94.

Yan, P., and Chen, D. F. (2009). *New geophysical evidence for gas hydrates in Baiyun Sag in the northern margin of the South China Sea.*

Yan, P., Wang, Y. L., Jin, Y. B., Zhao, M. X., and Zhong, G. J. (2021). Deep-water coral of multiple benthal strategies discovered from mounds in the Dongsha Waters in the South China Sea. *Earth Science Frontiers* 29 (4), 202–210. doi:10.13745/j.esf.sf.2022.1.13

Yan, P., Wang, Y. L., Zheng, H. B., Zhou, D. P., Chen, Z., et al. (2014). Geophysical features of mud volcanoes in the waters southwest of the Dongsha Islands. *Acta Oceanologica Sinica* 7, 142–148.

Yan, P., Wang, Y., Liu, J., Zhong, G., and Liu, X. (2017). Discovery of the southwest Dongsha Island mud volcanoes amid the northern margin of the South China Sea. *Marine and Petroleum Geology* 88 (3), 858–870. doi:10.1016/j.marpetgeo.2017.09.021

Yan, Y. N., Liao, J. P., Yu, J. H., Chen, C., Zhong, G., Wang, Y., et al. (2022). Velocity structure revealing a likely mud volcano off the Dongsha Island, the northern South China sea. *Energies* 15, 195. doi:10.3390/en15010195

Yang, S. C., Tong, Z. G., He, Q., Hao, J. R., et al. (2008). Mesozoic hydrocarbon generation history and igneous intrusion impacts in chaoshan depression, South China sea: A case of LF35-1-1 well. *China Offshore Oil and Gas* 20 (3), 152–156.

Zhang, J. Y., Sun, Z., and Zhang, S. F. (2014). Analysis of mesozoic tectonic deformation in the chaoshan depression of Pearl River Mouth Basin. *Journal of Tropical Oceanography* 33 (5), 41–49.

Zhang, L., Geng, A. S., Wang, L. L., Liao, Y., Xu, G., and Wei, Z. (2012). Assessment of mesozoic source rocks at the margin of South China continent. *Marine Geology & Quaternary Geology* 32 (1), 99–108. doi:10.3724/sp.j.1140.2012.01099

Zhang, Q. L., Zhang, H. F., Zhang, X. T., and Yang, L. L. (2018). The upper Cretaceous prototype basin of the Chaoshan depression in the northern South China Sea and its tectonic setting. *Chinese Journal of Geophysics* 61 (10), 4308–4321.

Zhao, S. J., Wu, S. G., Shi, H. S., Dong, D. D., Chen, D. X., Wang, R., et al. (2012). Structures and dynamic mechanism related to the Dongsha movement at the northern margin of South China Sea. *Progress in geophysics* 27 (3), 1008–1019. doi:10.6038/j.issn.1004-2903.2012.03.022

Zhong, G. J., Wu, S. M., and Feng, C. M. (2011). Sedimentary model of mesozoic in the northern South China sea. *Journal of Tropical Oceanography* 30 (1), 43–48.

Zhong, G. J., Yi, H., Lin, Z., Jin, H. F., and Liu, Z. H. (2007). Characteristic of source rocks and mesozoic in continental slope area of northeastern the south China sea and east Guangdong of China. *Xinjiang Petroleum Geology* 28 (6), 676–680.

Zhong, G. J., Zhang, R. W., Yi, H., Feng, C. M., and Zhao, Z. Q. (2018). The characteristics of shallow gas reservoir developed in the northern continental slope of South China Sea. *Journal of Tropical Oceanography* 37 (3), 80–85.

Zhou, D., Chen, H. Z., Sun, Z., Xu, H. H., et al. (2005). Three Mesozoic sea basins in the eastern and southern South China Sea and their relation to Tethys and Paleo-Pacific domains. *Journal of Tropical Oceanography* 24 (2), 16–25.

Zhou, D. (2002). Mesozoic strata and sedimentary environment in SW Taiwan Basin of NE South China sea and peikang high of Western taiwan. *Journal of Tropical Oceanography* 21 (2), 50–57.

Zhou, D., Yan, J. X., Qiu, Y. X., Chen, H. Z., and Sun, Z. (2003). Rout for the eastern extension of meso-tethys in the Western environs of the south China sea. *Earth Science Frontiers* 10 (4), 469–476.